

Surface chemistry analysis of lithium conditioned NSTX graphite tiles correlated to plasma performance



C.N. Taylor^{a,b,*}, K.E. Luitjohan^a, B. Heim^{a,b}, L. Kollar^a, J.P. Allain^{a,b}, C.H. Skinner^c,
H.W. Kugel^c, R. Kaita^c, A.L. Roquemore^c, R. Maingi^d

^a Purdue University, School of Nuclear Engineering, West Lafayette, IN 47906, USA

^b Birck Nanotechnology Center, Discovery Park, West Lafayette, IN 47907, USA

^c Princeton Plasma Physics Laboratory, Princeton, NJ 08543, USA

^d Oak Ridge National Laboratory, Oak Ridge, TN 37831, USA

ARTICLE INFO

Article history:

Received 18 October 2012

Received in revised form 22 July 2013

Accepted 24 September 2013

Available online 18 October 2013

PACS:

82.80.pv (Electron Spectroscopy)

52.55.Rk (Divertors)

79.20.Rf (Sputtering)

52.40.Hf (Plasma–material interactions)

Boundary layer physics

Keywords:

Lithium

Deuterium

Retention

Carbon-facing components

Divertor

X-ray photoelectron spectroscopy

Plasma–surface interactions

ABSTRACT

Lithium wall conditioning in NSTX has resulted in reduced divertor recycling, improved energy confinement, and reduced frequency of edge-localized modes (ELMs), up to the point of complete ELM suppression. NSTX tiles were removed from the vessel following the 2008 campaign and subsequently analyzed using X-ray photoelectron spectroscopy as well as nuclear reaction ion beam analysis. In this paper we relate surface chemistry to deuterium retention/recycling, develop methods for cleaning of passivated NSTX tiles, and explore a method to effectively extract bound deuterium from lithiated graphite. Li–O–D and Li–C–D complexes characteristic of deuterium retention that form during NSTX operations are revealed by sputter cleaning and heating. Heating to $\sim 850^\circ\text{C}$ desorbed all deuterium complexes observed in the O 1s and C 1s photoelectron energy ranges. Tile locations within approximately ± 2.5 cm of the lower vertical/horizontal divertor corner appear to have unused Li–O bonds that are not saturated with deuterium, whereas locations immediately outboard of this region indicate high deuterium recycling. X-ray photo electron spectra of a specific NSTX tile with wide ranging lithium coverage indicate that a minimum lithium dose, 100–500 nm equivalent thickness, is required for effective deuterium retention. This threshold is suspected to be highly sensitive to surface morphology. The present analysis may explain why plasma discharges in NSTX continue to benefit from lithium coating thickness beyond the divertor deuterium ion implantation depth, which is nominally <10 nm.

© 2013 Elsevier B.V. All rights reserved.

1. Introduction

Tokamak wall coatings have been employed [1] in fusion devices for many years to improve plasma performance, and to manage the intense plasma–wall interactions at the plasma facing surface. The use of low-Z coatings, lithium in particular, has been growing [2–7]. Lithium wall conditioning has improved plasma performance in TFTR [3], CDX-U [8], FTU [9], DIII-D [10], TJ-II [6], EAST [7], and NSTX [11,12].

Lithium conditioning represents a significant focus of the scientific program in the National Spherical Torus Experiment (NSTX). Lithium was first introduced into the NSTX in 2004 via pellet injection, with measurable but transient effects on the discharge

characteristics [13]. A lithium evaporator (LiTER) was installed in 2006 to increase lithium coverage by evaporating lithium onto the lower portion of NSTX, i.e. the lower divertor region, between discharges. Controlled experiments demonstrated reduced recycling, improved energy confinement time τ_E , and a reduction of edge instabilities known as edge localized modes (ELMs) [14]. In 2008, a second LiTER was installed into NSTX, toroidally displaced from the first unit to provide more complete coverage of the lower divertor and minimize shadowed regions [11,15].

To examine the correlation of plasma performance and ELM frequency on the amount of lithium evaporated between discharges, i.e., the lithium ‘dose’, lithium was systematically introduced into a series of discharges [16] with Type I ELMs. A gradual suppression of ELMs and improvement in performance was observed with increasing lithium dose; density profile modification due to reduced recycling [17,18] and edge transport [19] changed the edge pressure gradient, stabilizing the kink/peeling modes thought to be responsible for those ELMs.

* Corresponding author. Present address: Fusion Safety Program, Idaho National Laboratory, P.O. Box 1625, Idaho Falls, ID 83415-7113, USA. Tel.: +1 208 533 4068.

E-mail address: chase.taylor@inl.gov (C.N. Taylor).

Subsequent analysis [12] of that discharge sequence showed that the plasma characteristics changed nearly continuously with the lithium dose. A calculation using the TRIM code showed that the expected ion implantation depth ($E_i \leq 200$ eV) in the NSTX divertor was <10 nm, i.e. less than the minimum nominal lithium dose applied in the experimental sequence [20]. In other words, a saturation of the benefits of lithium was expected once the nominal lithium thickness exceeded the implantation range, but this was not observed. In this paper, our analysis of the complex lithium–carbon–oxygen–deuterium chemistry of NSTX tiles from that experimental campaign indicates that a lithium dose equivalent of much higher than the 10 nm deuterium implantation range is needed to saturate the plasma improvements described above.

In addition to wall conditioning, numerous parameters affect plasma discharge performance. For example, high performance (H-mode) plasma configurations typically utilize a high-triangularity shape which positions the inner strike point (ISP) on the vertical wall of the center stack and the outer strike point (OSP) on the inner horizontal divertor floor. This configuration positions the characteristic high-flux scrape off layer (SOL) on the lower horizontal divertor and may contribute to the unusual surface chemistry observed in Section 3. Examples of several plasma configurations are represented in Fig. 1. Throughout an experimental campaign, the strike-points, and consequently the private flux region (PFR) bounded by the strike-points, is positioned at various radial locations contributing to non-uniform “plasma processing” of the lower divertor. Since the strike-point locations and resulting PFR can vary so dramatically, we generalize the term “PFR samples” to refer to samples taken from approximately ± 5 cm of the lower horizontal divertor/center stack intersection (corner).

In addition to these parameters, plasma and surface properties are governed by individual experimental designs, and may include glow discharges (GDC), divertor seeding [21], wall conditioning (i.e., boronization [22], lithiumization [8,13,23,24], vessel baking, etc.), or a variety of other processes that modify the surface [1,25]. Over the course of an experimental campaign, thousands of individual plasma discharges (the 2008 campaign had 2427) use numerous plasma configurations [26]. Thermal and ion-induced diffusion result in atomic mixing of the near surface. Thus, by the end of a campaign, graphite tile and plasma facing component (PFC) surfaces represent a time-integrated surface that blends the plasma–wall interactions from many individual plasma discharges. Despite these variations we find consistent and systematic behavior that allow us to correlate offline laboratory experiments to tokamak PMI effects.

In a previous study, deuterium interactions with laboratory prepared lithiated-graphite samples were investigated using X-ray photoelectron spectroscopy (XPS) [27]. Salient peaks corresponding to deuterium interactions with lithiated graphite were identified as Li–O–D interactions and were observed at a binding energy of 533.0 eV in the XPS spectrum. In addition, deuterium interactions with lithiated graphite were also manifest in the C 1s spectrum as Li–C–D interactions and were positioned at 291.2 eV. Atomistic simulations corroborate these findings and suggest that oxygen plays the key role in lithium-aided deuterium retention [28]. Indeed, the majority of the present analysis focuses on the O 1s energy region because of these simulation results and experimentally the O 1s region was found to be very sensitive to lithium conditioning and deuterium irradiation. These laboratory spectra were then compared with spectra from NSTX tile analyses. The primary finding [27] was that after removing the passivated layer formed during air exposure, the NSTX tile samples revealed photoelectron spectra that aligned remarkably well with the spectra obtained from the controlled laboratory experiments. The close agreement in the spectra showed that controlled laboratory experiments are capable of replicating the plasma–surface interactions

that occur within NSTX, and furthermore, may be used to conduct experiments that may not be feasible in a fusion device.

This paper examines the surface chemistry of lithiated NSTX graphite tiles that were removed from various regions within NSTX, and discusses how tile surface chemistry is modified by NSTX conditioning and plasma–surface interactions based on their locations within vessel. Section 2 discusses the experimental setup and procedures; Section 3 describes the development of cleaning procedures and investigates the surface chemistry of the lower divertor in detail as well as the implications on performance within NSTX; Section 4 discusses changes in surface chemistry with increasing lithium dose; to conclude we summarize results and describe their relevance to plasma performance within NSTX.

2. Experimental setup

In 2007, prior to the start of the 2008 Experimental Campaign, the graphite tiles were cleaned manually using ScotchBrite™ abrasive pads, then washed with deionized water, and finally washed with ethanol. In November 2007, the vessel was then evacuated, and the graphite PFCs were baked up to 350 °C for 2 weeks, during which the outer vessel was baked at 150 °C, and then cooled to room temperature by the end of December 2007. In January 2008, a boronization was performed using 10 g of deuterated trimethyl-boron (TMB). Then 2 h of helium glow discharge (HeGDC) was applied, and NSTX plasma operations started. Thereafter, HeGDC was applied for 10 min between all discharges until LITER operations were started. Additional TMB boronizations were applied at a rate of about every 1–2 weeks, for a total of 9 applications in decreasing amounts from 10 g to 5 g per application, until April 2008. The total deposited TMB was 60 g. Thereafter, LITER operations started. Lithium was evaporated between discharges at rates ranging from 100 to 700 mg during the 10 min between discharges, depending on the experimental requirements. Varying durations of HeGDC were applied before LITER evaporation began. The total lithium deposition during the 2008 Experimental Campaign was 184 g.

Following the 2008 campaign, four NSTX tiles were removed prior to the typical cleaning procedure and shipped to Purdue University and Sandia National Laboratory for analysis. Three tiles were taken from the lower divertor and lower center stack as shown in Fig. 2(a) and the fourth was from the upper vessel as shown in Fig. 2(b). Tiles were exposed to air upon venting NSTX and supplemented by a humidifier to speed up passivation of the surface lithium. The tiles are 5.1 cm thick and made from Union Carbide ATJ graphite. A hole saw was used to extract several 1 cm diameter core samples from the tiles. The sample cores were analyzed by Purdue University and the tiles were analyzed by Sandia National Laboratory. The non-plasma-facing side of the tile samples were filed down to a sample height of ~ 2 –3 mm. Pressurized argon gas was used to remove any debris from the plasma-facing surface resulting from tile coring/sample preparation. The lower horizontal divertor tile A408-002 was a particularly interesting tile due to unexpected observed surface chemistry, and many additional samples were cored for analysis.

The tile samples were loaded into an ultra-high vacuum (UHV) chamber and subsequently analyzed “as-is” using XPS. The sample was exposed to Al K α X-rays (1486.6 eV) produced from a non-monochromatic, dual anode X-ray source, and photoelectrons ejected from the sample were analyzed using a seven-channel, energy selective Omicron hemispherical analyzer with a calibration accuracy of ± 0.6 eV [29]. Repeated XPS scans show insignificant random error, and the overall error for XPS peak positions is ± 0.6 eV. Sputtering and heating were conducted in a “preparation” chamber that is connected to the “analysis” chamber via isolation

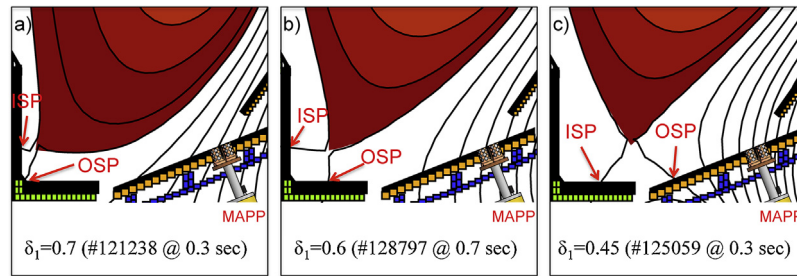


Fig. 1. Plasma configurations showing the inner and outer strikepoint locations for (a) high-elongation (high delta), (b) medium-elongation, and (c) low-elongation plasma configurations. The private flux region (PFR) is contained between the inner strikepoint (ISP) and outer strike point (OSP). The materials analysis particle probe (MAPP) is discussed in Section 3.1 and Ref [31].

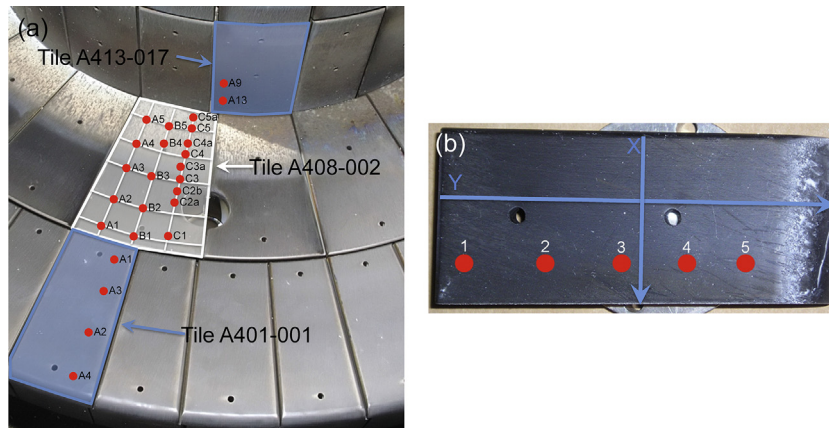


Fig. 2. NSTX tiles from 2008 experimental campaign that were cored and analyzed at Purdue University. (a) Tiles A401-001, A408-002, and A413-017 were removed from the lower horizontal divertor and lower vertical divertor (center stack). Gray and white panes are used in subsequent figures to distinguish data when multiple tiles are compared simultaneously. (b) Tile A235-021 was removed from upper portion of the vessel near LiTER. Arrows show direction of scan for ion beam analysis. Numbered circles show approximate location of cored samples.

valves. Argon sputtering was performed using an Omicron ISE-10 ion gun. Irradiation was typically conducted at 1 keV with a flux of $2.5 \times 10^{13} \text{ cm}^{-2} \text{ s}^{-1}$. Sample heating is performed using a resistive tungsten filament heater with a heating ramp rate of $\sim 1^\circ \text{ C s}^{-1}$. XPS was performed after each process (e.g. sputtering, heating) to analyze changes in surface chemistry.

Ion beam analysis was conducted in parallel at Sandia National Laboratory on the tiles from which cores were extracted for the XPS analysis. The $\text{Li}^7(\text{H}^1, \alpha)\alpha$ nuclear reaction was used to measure the lithium areal density and has a probing depth of about 15 μm . The deuterium coverage was measured using the $\text{D}^3(\text{He}, \text{p})\alpha$ nuclear reaction that has a probing depth of about 7 μm (these probing depths are based on a graphite mass density of 2 g cm^{-3}). The depth resolution for both techniques is $\sim 1 \mu\text{m}$ full width half max (FWHM), and the ion beam spot size is approximately 1 mm^2 . Full experiment parameters and details were reported elsewhere [30].

3. Results and discussion

3.1. Lower divertor radial dependence on the tile surface chemistry

An XPS survey scan of the lower divertor tiles is shown in Fig. 3. Distinct trends are visible in the form of broad, non-Gaussian peaks in the O 1s, C 1s, and Li 1s energy ranges in the top four curves. XPS spectra were collected from as-received lower horizontal divertor and center stack (lower vertical divertor) NSTX tile samples. Tile A413-017 was removed from the lower center stack, Tile A408-002 from the inner-most lower horizontal divertor tile, and

A401-001 from the location radially adjacent to tile A408-002. Fig. 2(a) shows a photo of the lower divertor section that includes these tiles. The characteristic peaks associated with Li–O–D and Li–C–D found during laboratory experiments were not expected from these as-received tiles since they had been exposed to air prior to analysis. The vertical dashed lines in Fig. 3 are added to reference known interactions for lithiated graphite after deuterium exposure [27,29].

Samples taken from near the corner, where tile A413-017 and tile A408-002 meet, show broad non-Gaussian XPS peaks. In Fig. 3, the divertor corner would be located at the intersection of the top gray-background panes and the white-background panes. The notable feature in these as-is spectra is that the peaks appear to be symmetric about the corner, and the unusual broad peaks in this region correspond to the geometry of a medium-elongation PFR (Fig. 1(b)).

An in situ PMI diagnostic, such as the Materials Analysis Particle (MAPP) will be capable of discerning whether the source of the unusual PFR chemistry is a result of high lithium coverage, air exposure, high deuterium flux, high temperature, or some other influence that is affected by performing an ex situ analysis [31]. More importantly, MAPP will act as a prompt diagnostic that will directly connect plasma performance to tile chemistry immediately following a plasma discharge.

3.2. Tile cleaning

The as-is samples from each of the four NSTX tiles were cleaned in various steps. Key sample parameters including core location,

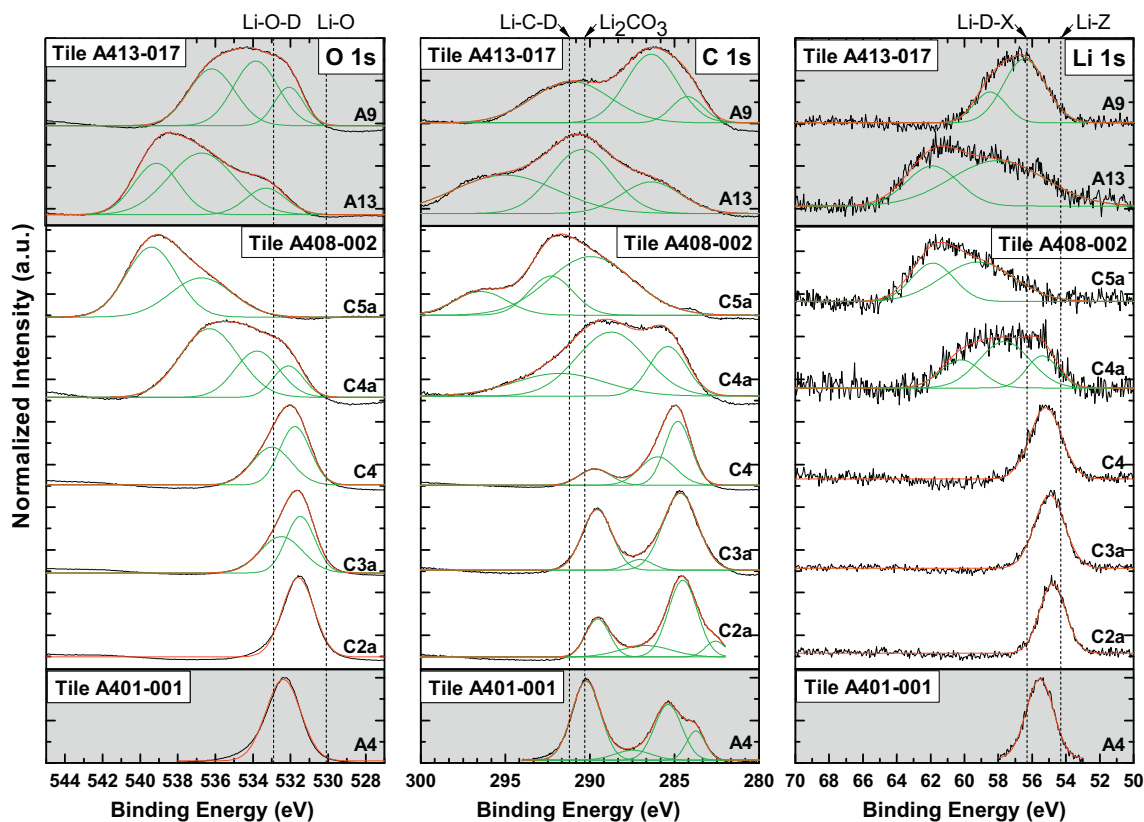


Fig. 3. (a) O 1s (b) C 1s, and (c) Li 1s spectra of select as-received tile samples. Spectra appearance varies based on location on divertor floor. The shaded and white panes represent distinct tiles, and the traces in a pane are collected from various sample locations within that tile.

Ar sputtering time, and maximum heating temperatures are summarized for these samples in Table 1. The black curves in Fig. 4 represent the as-received sample; red curves show the sample following the first cleaning step, Ar sputtering; blue curves follow heating. Ar sputtering successfully removes the passivated layer for most, but not all samples. For example, sputter cleaning did not reveal deuterium related peaks for samples in the lower divertor nearest the corner (samples A5 and C4a). Samples A5 and C4a in Fig. 4 show that Ar sputtering alters the broad,

Table 1

Summary of NSTX post-mortem core tiles and samples from this analysis. Tile A235-021 was removed from the upper vessel near LiTER, tile A413-017 was removed from the lower center stack, and tile A408-002 and A401-001 were removed from the lower divertor. Tiles A413-017 and A408-002 from the corner between the center stack and lower divertor, respectively.

Tile	Core Sample	Distance from corner	Sputtering time	Heating temperature
A235-021	2	NA	7 h	NA
	5	NA	7 h	573 °C
A413-017	A9	4.6 cm ^a	3 h	531 °C
	A13	2.1 cm ^a	3 h	531 °C
A408-002	C5a	0.6 cm	1 h	564 °C ^b
	C5	2.1 cm	0 h	NA
	A5	2.2 cm	3 h	582 °C
	C4a	3.5 cm	2 h	546 °C
	C4	4.9 cm	0 h	NA
	C3a	6.2 cm	0 h	NA
	C2a	9.3 cm	0 h	NA
A1	13.1 cm	3 h	845 °C	
A401-001	A4	25.1 cm	3 h	587 °C

^a Distance up the center stack where 0 cm is the divertor surface.

^b Sample was heated to ~350, 450, and 550 °C prior to Ar sputtering.

non-Gaussian spectra; however, the post-sputtered spectra remain as un-decipherable as the pre-cleaned spectra. Following Ar sputtering, samples A5 and C4a were annealed (heated) to ~550 °C, and the resulting XPS spectra change dramatically. Following sputtering and heating, sample A5 clearly shows two prominent O 1s peaks positioned at 529.8 eV and 532.7 eV. These peaks correspond to Li–O and Li–O–D chemical interactions [27,29].

For these two samples (A5 and C4a), Ar sputtering alone resulted in subtle shifts, which indicates that sputtering eventually may have been able to recover the buried deuterium chemistry if taken well beyond the fluences used in these experiments ($>7 \times 10^{17} \text{ cm}^{-2}$). However, surface recovery time is greatly reduced by applying a procedure that includes both sputtering and heating to ~550 °C. Therefore, we recommend that fusion devices which need to recover from air exposure or wall passivation apply a cleaning procedure of sputtering (glow discharge with wall fluence $\geq 5 \times 10^{21} \text{ m}^{-2}$) and then heating.

Table 2

Summary of peak positions found in controlled laboratory experiments where lithiated graphite samples were bombarded with deuterium, compared to NSTX tile A235-021 sample 5 following Ar sputter cleaning.

Photoelectron energy region	Peak location in laboratory experiments	Peak location in post cleaned NSTX tile A235-021	Interaction groups
O 1s	530.0 eV	530.0 eV	Li–O
	532.9 eV	533.1 eV	Li–O–D
C 1s	285.1 eV	284.8 eV	Graphitic
	291.2 eV	291.3 eV	
Li 1s	54.8 eV	54.7 eV	Li–Z
	56.3 eV	56.3 eV	Li–D–X

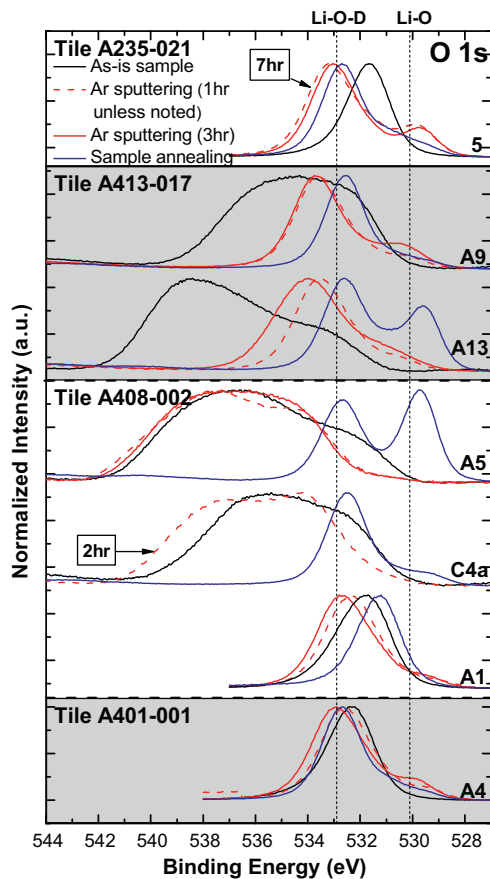


Fig. 4. O1s X-ray photoelectron spectra for NSTX tile core samples as received (black), after Ar cleaning (red), and after sample annealing (blue). The shaded and white panes represent distinct tiles, and the traces in a pane are collected from various sample locations within that tile. The two samples outward from the divertor corner (A5 and C4a) required Ar sputtering and heating ($\sim 550^\circ\text{C}$) to uncover the Li–O–D and Li–C–D peaks characteristic of deuterium retention. Sample A1 shows uncovering of D-related peaks with sputtering alone. High temperature heating of sample A1 ($\sim 850^\circ\text{C}$) eliminates Li–O–D and Li–C–D interactions in the O 1s and C 1s regions. (For interpretation of the references to color in this figure legend, the reader is referred to the web version of the article.)

The spectra from cleaned samples are similar in appearance to those found in laboratory experiments and the measured peak energies are within 0.5 eV of peaks identified as Li–O–D and Li–C–D interactions (compared to our 0.6 eV XPS error; see Table 2). This illustrates the utility of offline laboratory experiments in elucidating tokamak plasma–surface interactions. It remains unclear why samples taken from within the average PFR required additional cleaning steps in order to reveal deuterium related XPS peaks. Ion beam analysis from Fig. 5 shows that these samples have relatively large amounts of lithium, although this behavior is not consistent for all samples with comparable lithium coverage. Likewise, this trend is not found to be linked with deuterium coverage or other surface impurities detected by XPS. The broad, non-Gaussian peak shape and position was not reproducible in offline laboratory experiments through a series of heating, ion bombardment, air and impurity exposures. Presently, the only known unique characteristic of samples with broad spectra is that they originated in the lower horizontal divertor tiles near the corner and may be attributed to unique plasma processing resultant from high ion flux in combination with high surface temperature.

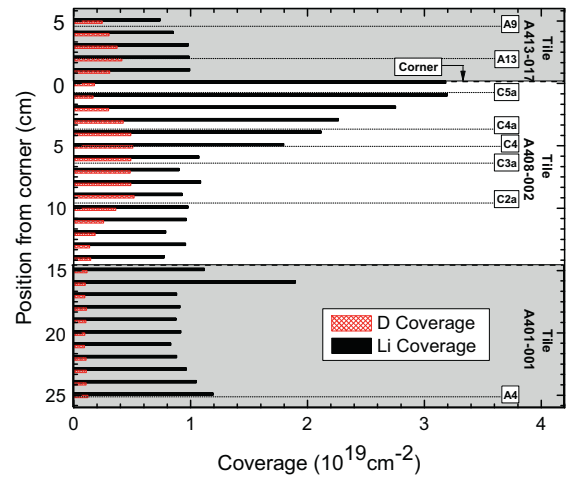


Fig. 5. Nuclear reaction ion beam analysis (IBA) of 2008 NSTX post-mortem tiles. Deuterium and lithium coverage is represented for several tiles in 1 cm increments. The shaded and white panes represent distinct tiles, and the traces in a pane are collected from various sample locations within that tile.

3.3. Deuterium saturation

Deuterium saturation of lithiated graphite can be observed in the lower divertor tile surface chemistry by comparing the relative height of the Li–O–D peak with the Li–O peak height. In previous experiments [29], deuterium saturation was observed as the Li–O–D/Li–O peak ratio increased and stabilized with increasing deuterium fluence ($\sim 5 \times 10^{17} \text{ cm}^{-2}$), indicating that Li–O is consumed and converted into Li–O–D as more deuterium is introduced.

In Fig. 4, the Li–O–D peak (blue, see left-most dotted vertical line) dominates for all samples, with the exception of the two samples nearest the corner. The prominence of the Li–O–D peaks in these samples and lack of the Li–O suggests that these locations were regularly saturated with deuterium. However, samples A13 and A5 are found to have prominent Li–O peaks, indicating that they were *not* saturated with deuterium. We conjecture that during the 2008 campaign, regions within ± 2.2 cm of the lower divertor corner had persistent unused capacity to pump deuterium, while surrounding divertor locations were, on average, saturated with deuterium. Furthermore, these saturated locations were likely primary localized sources of deuterium recycling.

These observations have two immediate implications on plasma operations. First, since cumulative sputtering reveals more Li–O, we can conjecture that the lithium deposited from earlier NSTX discharges was not fully utilized and had remaining capacity to retain deuterium and form Li–O–D. The second implication concerns hydrogen inventory [32]. That is, these results show that Li–O–D remains on the surface and does not intercalate as readily and deeply as lithium does. The near-surface hydrogen bond facilitates the use of the various tritium removal techniques that have been explored in other devices [33].

3.4. High temperature annealing

If a sample is heated excessively, deuterium complexes are effectively desorbed. Sample A1 from NSTX tile A408-002 in Fig. 4 underwent 3 h Ar sputtering followed by sample heating to 845°C . XPS spectra after this high temperature heating sequence are void of all known deuterium related interactions in the O 1s and C 1s energy ranges. This significant finding demonstrates that deuterium can effectively be released from lithiated graphite by heating to $\leq 845^\circ\text{C}$.

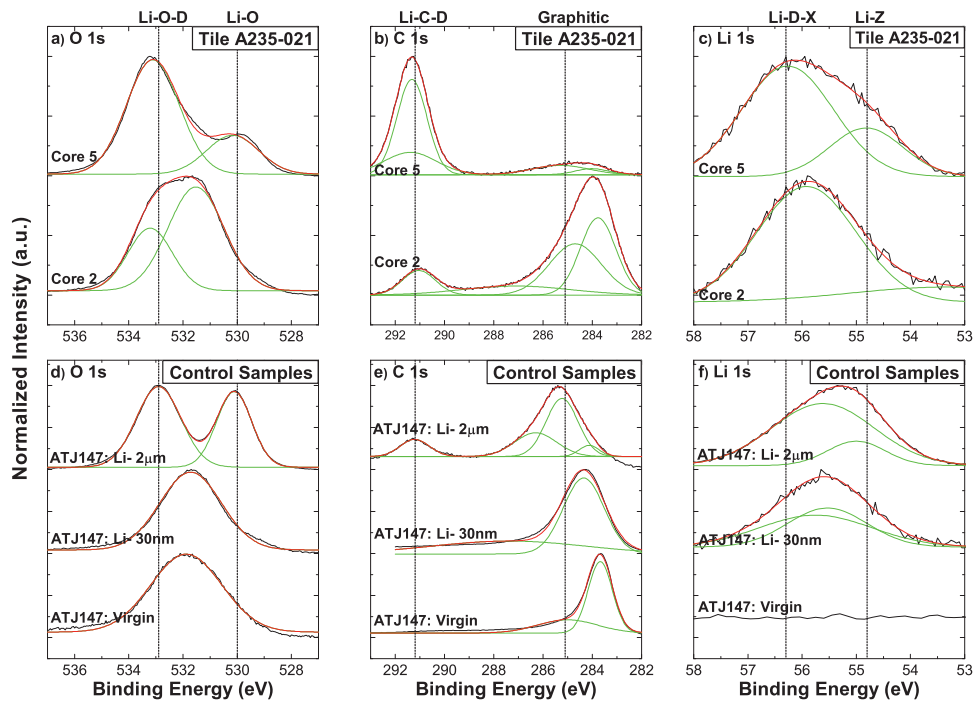


Fig. 6. Comparison of NSTX tile A235-021 (top frames) with control samples (bottom frames). For NSTX tile A235-021, core sample 2 corresponds to a region of low lithium coverage and core sample 5 corresponds to a region of high lithium coverage, both after 7 h Ar cleaning. Control samples show virgin spectra, low lithium dose of 30 nm, and a high lithium dose of 2 μm .

Although after high temperature heating the sample is void of known deuterium related XPS peaks, the spectra do not align precisely with that of lithiated graphite, therefore it cannot be assumed that high temperature heating perfectly restores the sample to be lithiated graphite. Instead, after being heated to 845 $^{\circ}\text{C}$, this sample more closely resembles the spectra obtained from sample ATJ113 with low lithium coverage (30 nm), as will be discussed in Section 4 and shown in Fig. 6.

During the heating sequence, a line-of-sight quadrupole mass spectrometer (QMS) was used to monitor the emission species. High emission ($>2 \times 10^{-5}$ Torr) was observed from amu 28 and 44, which correspond to N_2 and CO_2 molar masses, and masses 18 (H_2O) and 16 (O_2) both had an emission of $\sim 8 \times 10^{-7}$ Torr (compared to the chamber's base pressure of 5×10^{-9} Torr). Remarkably, however, at this high temperature lithium evaporation species ^6Li , ^7Li , $^6\text{Li}_2$, and $^7\text{Li}_2$ [34] did not exceed 4×10^{-7} Torr. Due to pure lithium's high vapor pressure of >0.1 Pa (7.5×10^{-5} Torr) at 450 $^{\circ}\text{C}$ [35], lithium applications and concepts in fusion devices have typically been limited to low wall temperature devices to avoid unacceptable lithium erosion/evaporation [36–41]. However, these results demonstrate that lithiated graphite behaves fundamentally different than pure lithium, and that excessive lithium evaporation may not be of significant concern for hot graphite walls ≤ 845 $^{\circ}\text{C}$.

4. Low vs. high-lithium coverage

Tile A235-021 was removed from the upper vessel, near LITER, and is of interest due to its diverse lithium coverage. Two samples (cores 2 and 5, see Fig. 2b) removed from this tile exhibit very different surface chemistry although both samples followed the same cleaning procedure. Fig. 6a shows the post cleaning spectra for core samples 2 and 5, as well as spectra from two samples produced in offline laboratory experiments. The cleaning procedure on sample 5 results in the clear separation of the Li–O–D and Li–O peaks in the

O 1s spectrum. These same two peaks are not observed using the identical cleaning process for sample 2. Deconvolution of the O 1s spectrum for core sample 2 suggests that the peak is comprised of two smaller peaks, one of which aligns with Li–O–D. Likewise, differences are observed between the two samples in the C 1s and Li 1s energy ranges. In the C 1s energy range for sample 2, the graphitic peak is dominant and the smaller peak at ~ 291.2 eV aligns with the peak identified as Li–C–D. In the Li 1s range, the presence of lithium is observed and the peak shape appears to be similar to that of sample 5.

The most striking difference between the two spectra is in the O 1s range. During typical experiments, two peaks are regularly observed in the O 1s spectrum at ~ 530 and 533 eV corresponding to Li–O and Li–O–D interactions, respectively, after deuterium irradiation of a lithiated graphite sample. What makes this tile peculiar is that sample 2 is separated from sample 5 by only 14.0 cm, yet XPS results show differing surface chemistry.

Ion beam analysis (IBA) was performed on tile A235-021 after each of the 2006–2009 campaigns [30,42]. Scans were taken in the toroidal and poloidal directions through the center of the tile in 1 cm intervals. Fig. 7 shows the lithium coverage of the tile following each of the four campaigns. The general multi-year trend for this tile is that the lithium coverage is dramatically higher at the end of the tile in the y-direction, and for the 2008 tile, sample 5 had 45% more lithium than sample 2. Thus, core sample 2 represents a region of low net lithium coverage, and core sample 5 represents a region of high net lithium coverage. IBA results show near uniform deuterium coverage over the tile, therefore, uneven lithium coverage is suspected to be the cause of the differences in spectra between the two core samples.

Spectra in Fig. 6(d–f) show results from laboratory experiments showing three cases: virgin ATJ graphite, and ATJ graphite samples with lithium doses of 30 nm and 2 μm equivalent thickness, respectively. Lithiated samples were then irradiated with 500 eV/amu deuterium to a fluence of $\sim 9 \times 10^{16}$ cm^{-2} . The virgin graphite case is presented as a reference to compare with the low lithium case.

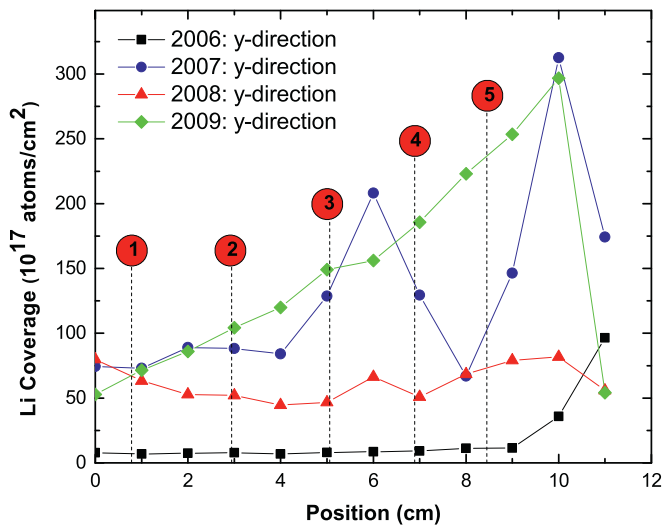


Fig. 7. Ion beam analysis showing lithium concentration for NSTX tile A235-021 after the FY 2006, 2007, 2008 and 2009 campaigns. Numbered circles show the approximate location for core samples in Fig. 2(b). For the 2008 tile, location 5 had 45% more lithium than location 2. (Lines to guide the eye).

A Li 1s peak is present for the low lithium case (30 nm) as well as the high lithium case (2 μm). In the O 1s region, no significant differences are observed between virgin graphite and the D-irradiated sample with a 30 nm lithium dose. More importantly, following deuterium irradiation, Li–O–D interactions at 533.0 eV are *not* observed. For the sample with 2 μm lithium, two peaks *do* form that correspond to Li–O–D and Li–O interactions [27]. Similarly, the interaction of deuterium is not observed in the C 1s spectrum (Fig. 6(e)) for a 30 nm Li dose. Although 30 nm Li is present, since the only nominal difference between the two samples is the lithium dose, the lack of Li–O–D and Li–C–D peaks should be a result of lithium deprivation. We deduce that a minimum lithium dose exists for which effective deuterium bonding can occur and produce the characteristic Li–O–D and Li–C–D interactions that are observed in both NSTX tiles and offline laboratory experiments.

Pinpointing an exact threshold lithium dose that will enable deuterium bonding is impractical due to surface intercalation and morphology. Lithium readily intercalates into graphite [27,43]. For this reason, lithium doses cannot be considered as films on top of a flat substrate and therefore are identified as nominal thicknesses. ATJ graphite samples in these experiments are polished with sub-micron polish paper, yet surface roughness is on the order of microns. Sample roughness effectively thins the deposited film. The effects of morphology could be reduced in laboratory experiments by using alternate carbon allotropes such as highly oriented pyrolytic graphite (HOPG), or amorphous carbon (a-C) films. We have observed Li–C–D interactions at a lithium dose of 100 nm, however the Li–O–D peak was absent. Li–O–D has been observed with a lithium dose of 500 nm [44].

The results from this upper vessel tile point to a phenomenon with implications on global plasma performance; indeed, a direct dependence on increasing lithium dose and plasma performance. XPS spectra from NSTX tile and laboratory control samples with high lithium coverage show deuterium bonding, thus indicative of deuterium retention, whereas the samples with low lithium coverage were absent of prominent deuterium bonding. On a global scale, if the entire NSTX vessel had “low” lithium coverage, then one would expect little effect on plasma performance. Maingi et al. demonstrated [12] continuous plasma improvements in NSTX discharges as the first amounts of lithium were systematically introduced during the 2009 campaign until several grams of lithium

were evaporated onto the PFCs. The improvements became more pronounced after several evaporations (each of which was nominally at least 30–125 nm) and continued well beyond the <10 nm ion range thus demonstrating the effects of a lithium response threshold. This is consistent with the above XPS results showing a threshold in the 100–500 nm range.

5. Conclusions

Four NSTX post-mortem tiles were removed from the vessel and 1 cm core samples were extracted from various locations in the tiles. Core samples were analyzed using X-ray photoelectron spectroscopy. Tiles passivate upon air exposure when removed from NSTX. Sputtering and heating procedures have been established to remove and repair the passivated layer in order to uncover the Li–O–D (532 eV) and Li–C–D (291.2 eV) interactions that developed during NSTX plasma discharge operation. The cleaning procedure consists of Ar sputtering (1 keV, fluence $>9 \times 10^{16} \text{ cm}^{-2}$) followed by sample annealing to $\sim 550^\circ\text{C}$. Some samples revealed Li–O–D and Li–C–D interactions through sputtering alone. However, several samples removed from locations closest to the lower divertor/center stack (corner) intersection exhibit broad, non-Gaussian photoelectron spectra that could not be cleaned through Ar sputtering alone. We conjecture that a combination of high heat and high ion flux from the scrape off layer plasma-processed these samples in a manner that controlled laboratory experiments were not able to replicate. Ion sputtering *and* heating removes/repairs this surface layer and is manifest by the characteristic Li–O–D and Li–C–D XPS peaks. Sputtering prior to heating is found to expedite the passivation removal and is the recommended procedure for fusion devices and laboratory experiments to clean passivated lithiated-graphite. Excessive heating to 850°C effectively desorbs all Li–O–D and Li–C–D bonds observed in the photoelectron O 1s and C 1s energy regions, and could be a method for controlling tritium inventory.

A comparison of the relative intensity of the Li–O and Li–O–D XPS peaks from lower divertor samples provides information regarding local deuterium recycling and retention. Samples within approximately ± 2.5 cm of the center stack/lower divertor (corner) intersection had a prominent Li–O peak, which indicates these samples had remaining capacity to retain deuterium following the 2008 NSTX campaign. Samples beyond this region were completely absent of this Li–O peak and the Li–O–D peak dominated the O 1s spectrum. In previous studies this was an indication of deuterium saturation, which leads us to conjecture that *on average* these tile locations contributed to deuterium recycling rather than deuterium retention.

XPS performed on a tile from the upper vessel after our cleaning procedure reveals deuterium related interactions at the inner radial side of the tile and the absence of these deuterium related interactions on the outer radial side of the tile. Ion beam analysis identifies a large lithium-coverage gradient on this tile suggesting that low lithium coverage is correlated to the absence of deuterium related interactions (including the Li–O–D peak). Controlled experiments replicate this behavior for lithium doses below 500 nm *nominal* thickness and show that both Li–O–D and Li–C–D interactions are apparent after a minimum lithium dose of 100–500 nm is deposited. Since surface roughness can be much greater than these deposited lithium doses, this minimum dose is conjectured to be highly dependent on surface morphology. In addition, rapid lithium-graphite intercalation precludes these lithium doses from residing on the graphite surface as a film layer. These results suggest that the most effective lithium enhanced retention of deuterium occurs at nominal lithium doses ≥ 100 –500 nm in the high recycling regions in pre-lithium discharges, i.e., the lower divertor. This

thickness is well in excess of the ~ 10 nm ion implantation depth expected for NSTX divertor conditions. In the previously described experiment, the NSTX discharges continued to respond to minimum lithium dose up to 250–1000 nm film thickness, with no signs of saturation. The present work identifies the importance of the Li–O–D reaction in deuterium pumping, and the possible origin of the continuous dependence that was previously unexplained [12].

Acknowledgements

We would like to thank the Purdue University Graduate School for providing student funding, T. Morton for his contributions in running experiments and sample preparation, L. Guttadora at the Princeton Plasma Physics Laboratory for helping with sample core extraction. Work supported by US DOE Contract DE-FG02-08ER54990 and DE-AC02-09CH11466.

References

- [1] J. Winter, Wall conditioning in fusion devices and its influence on plasma performance, *Plasma Physics and Controlled Fusion* 38 (1996) 1503.
- [2] J.A. Snipes, E.S. Marmor, J.L. Terry, M.G. Bell, R.V. Budny, K.W. Hill, et al., Wall conditioning with impurity pellet injection on TFTR, *Journal of Nuclear Materials* 196 (1992) 686–691.
- [3] D.K. Mansfield, D.W. Johnson, B. Grek, H.W. Kugel, M.G. Bell, R.E. Bell, et al., Observations concerning the injection of a lithium aerosol into the edge of TFTR discharges, *Nuclear Fusion* 41 (2001) 1823.
- [4] M.L. Apicella, G. Mazzitelli, V. Pericoli-Ridolfini, V. Lazarev, A. Alekseyev, A. Vertkov, et al., First experiments with lithium limiter on FTU, *Journal of Nuclear Materials* 363–365 (2007) 1346–1351.
- [5] R. Majeski, R.P. Doerner, T. Gray, R. kaita, R. Maingi, D. mansfield, et al., Enhanced energy confinement and performance in a low-recycling tokamak, *Physical Review Letters* 97 (2006) 075002.
- [6] J. Sánchez, F.L. tabarés, D. Tafalla, J.A. Ferreira, I. García-Cortés, C. Hidalgo, et al., Impact of lithium-coated walls on plasma performance in the TJ-II stellarator, *Journal of Nuclear Materials* (2009) 1–6.
- [7] G.S. Xu, B.N. Wan, J.G. Li, X.Z. Gong, J.S. Hu, J.F. Shan, et al., Study on H-mode access at low density with lower hybrid current drive and lithium-wall coatings on the EAST superconducting tokamak, *Nuclear Fusion* 51 (2011) 072001.
- [8] R. Majeski, M. Boaz, D. Hoffman, B. Jones, R. kaita, H. Kugel, et al., Plasma performance improvements with liquid lithium limiters in CDX-U, *Fusion Engineering and Design* 65 (2003) 443–447.
- [9] A.A. Tuccillo, A. Alekseyev, B. Angelini, S.V. Annibaldi, M.L. Apicella, G. Apruzzese, et al., Overview of the FTU results, *Nuclear Fusion* 49 (2009) 104013.
- [10] G.L. Jackson, E.A. Lazarus, G.A. Navratil, R. Bastasz, N.H. Brooks, D.T. Garnier, et al., Enhanced performance discharges in the DIII-D tokamak with lithium wall conditioning, *Journal of Nuclear Materials* 241 (1997) 655–659.
- [11] M.G. Bell, H.W. Kugel, R. kaita, L.E. Zakharov, H. Schneider, B.P. LeBlanc, et al., Plasma response to lithium-coated plasma-facing components in the National Spherical Torus Experiment, *Plasma Physics and Controlled Fusion* 51 (2009) 124054.
- [12] R. Maingi, S.M. Kaye, C.H. Skinner, D.P. Boyle, J.M. Canik, M.G. Bell, et al., Continuous improvement of H-mode discharge performance with progressively increasing lithium coatings in the National Spherical Torus Experiment, *Physical Review Letters* 107 (2011) 145004.
- [13] H.W. Kugel, M.G. Bell, R. Bell, C. Bush, D. Gates, T. Gray, et al., Effect of lithium PFC coatings on NSTX density control, *Journal of Nuclear Materials* 363–365 (2007) 791–796.
- [14] H.W. Kugel, M.G. Bell, J.W. Ahn, J.P. Allain, R. Bell, J. Boedo, et al., The effect of lithium surface coatings on plasma performance in the National Spherical Torus Experiment, *Physics of Plasmas* 15 (2008) 056118.
- [15] H.W. Kugel, D. mansfield, R. Maingi, M.G. Bell, R.E. Bell, J.P. Allain, et al., Evaporated lithium surface coatings in NSTX, *Journal of Nuclear Materials* (2009) 1–5.
- [16] D.K. Mansfield, H.W. Kugel, R. Maingi, M.G. Bell, R. Bell, R. kaita, et al., Transition to ELM-free improved H-mode by lithium deposition on NSTX graphite divertor surfaces, *Journal of Nuclear Materials* 390–391 (2009) 764–767.
- [17] R. Maingi, T. Osborne, B. leblanc, R. Bell, J. Manickam, P. Snyder, et al., Edge-localized-mode suppression through density-profile modification with lithium-wall coatings in the National Spherical Torus Experiment, *Physical Review Letters* 103 (2009) 075001.
- [18] D.P. Boyle, R. Maingi, P.B. Snyder, J. Manickam, T.H. Osborne, R.E. Bell, et al., The relationships between edge localized modes suppression, pedestal profiles and lithium wall coatings in NSTX, *Plasma Physics and Controlled Fusion* 53 (2011) 105011.
- [19] J.M. Canik, R. Maingi, S. Kubota, Y. Ren, R.E. Bell, J.D. Callen, et al., Edge transport and turbulence reduction with lithium coated plasma facing components in the National Spherical Torus Experiment, *Physics of Plasmas* 18 (2011) 056118.
- [20] R. kaita, H.W. Kugel, T. Abrams, J.P. Allain, M.G. Bell, R.E. Bell, et al., Characterization of fueling NSTX H-mode plasmas diverted to a liquid lithium divertor, *Journal of Nuclear Materials* (2013).
- [21] V.A. Soukhanovskii, R. Maingi, D.A. Gates, J.E. Menard, S.F. Paul, R. raman, et al., Divertor heat flux mitigation in the National Spherical Torus Experiment, *Physics of Plasmas* 16 (2009) 022501.
- [22] C.H. Skinner, H.W. Kugel, R. Maingi, W.R. Wampler, W. Blanchard, M.G. Bell, et al., Effect of boronization on ohmic plasmas in NSTX, *Nuclear Fusion* 42 (2002) 329.
- [23] H. Sugai, H. Toyoda, K. Nakamura, K. Furuta, M. Ohori, K. Toi, et al., Wall conditioning with lithium evaporation, *Journal of Nuclear Materials* 220 (1995) 254–258.
- [24] B. Terreault, H.Y. Guo, D. Kéroack, R.W. Paynter, W.W. Zuzak, G. Abel, et al., Effect of lithium wall conditioning on deuterium in-vessel retention in the TdeV tokamak, *Journal of Nuclear Materials* 220 (1995) 1130–1134.
- [25] H.F. Dylla, A review of the wall problem and conditioning techniques for tokamaks, *Journal of Nuclear Materials* 93 (1980) 61–74.
- [26] D.A. Gates, J. Ahn, J. Allain, R. Andre, R. Bastasz, M. Bell, et al., Overview of results from the National Spherical Torus Experiment (NSTX), *Nuclear Fusion* 49 (2009) 104016.
- [27] C.N. Taylor, B. Heim, J.P. Allain, Chemical response of lithiated graphite with deuterium irradiation, *Journal of Applied Physics* 109 (2011) 053306–153306.
- [28] P.S. Krstic, J.P. Allain, C.N. Taylor, J. Dadrás, S. Maeda, K. Morokuma, et al., Deuterium uptake in magnetic-fusion devices with lithium-conditioned carbon walls, *Physical Review Letters* 110 (2013) 105001.
- [29] C.N. Taylor, J.P. Allain, B. Heim, P.S. Krstic, C.H. Skinner, H.W. Kugel, Surface chemistry and physics of deuterium retention in lithiated graphite, *Journal of Nuclear Materials* 415 (2010) S777–S780.
- [30] W.R. Wampler, C.H. Skinner, H.W. Kugel, A.L. roquemore, Measurement of lithium and deuterium on NSTX carbon tiles, *Journal of Nuclear Materials* (2009) 1–4.
- [31] C.N. Taylor, B. Heim, S. Gonderman, J.P. Allain, Z. Yang, R. kaita, et al., Materials analysis and particle probe: a compact diagnostic system for in situ analysis of plasma-facing components (invited), *Review of Scientific Instruments* 83 (2012) 10D703.
- [32] G. Federici, C.H. Skinner, J.N. Brooks, J.P. Coad, C. Grisolia, A.A. Haasz, et al., Plasma-material interactions in current tokamaks and their implications for next step fusion reactors, *Nuclear Fusion* 41 (2001) 1967.
- [33] C.H. Skinner, N. Bekris, J.P. Coad, C.A. Gentile, M. Glugla, Tritium removal from JET and TFTR tiles by a scanning laser, *Journal of Nuclear Materials* 313 (2003) 496–500.
- [34] K. Kimoto, I. Nishida, H. Takahashi, H. Kato, A study of lithium clusters by means of a quadrupole mass analyzer, *Japanese Journal of Applied Physics* 19 (1980) 1821–1828.
- [35] H. Sugai, M. Ohori, H. Toyoda, Lithium wall conditioning for fuel and impurity control, *Vacuum* 47 (1996) 981–984.
- [36] R. Bastasz, W. Eckstein, Plasma-surface interactions on liquids, *Journal of Nuclear Materials* 290 (2001) 19–24.
- [37] R.P. Doerner, M.J. Baldwin, R.W. Conn, A.A. Grossman, S.C. Luckhardt, R. Seraydarian, et al., Measurements of erosion mechanisms from solid and liquid materials in PISCES-B, *Journal of Nuclear Materials* 290 (2001) 166–172.
- [38] R.P. Doerner, M.J. Baldwin, S.I. Krashennnikov, D.G. Whyte, Behavior of high temperature liquid surfaces in contact with plasma, *Journal of Nuclear Materials* 313 (2003) 383–387.
- [39] J.N. Brooks, J.P. Allain, R. Bastasz, R.P. Doerner, T. Evans, A. Hassanein, et al., Overview of the ALPS program, *Fusion Science and Technology* 47 (2005) 669–677.
- [40] M.A. Abdou, A. Ying, N. Morley, K. Gulec, S. Smolentsev, M. Kotschenreuther, et al., On the exploration of innovative concepts for fusion chamber technology, *Fusion Engineering and Design* 54 (2001) 181–247.
- [41] R. Majeski, M. Boaz, D. Hoffman, B. Jones, R. kaita, H. Kugel, et al., CDX-U operation with a large area liquid lithium limiter, *Journal of Nuclear Materials* 313 (2003) 625–629.
- [42] W.R. Wampler, Private communication (2011).
- [43] N. Itou, H. Toyoda, K. Morita, H. Sugai, Rapid diffusion of lithium into bulk graphite in lithium conditioning, *Journal of Nuclear Materials* 290 (2001) 281–285.
- [44] J.P. Allain, C.N. Taylor, Lithium-based surfaces controlling fusion plasma behavior at the plasma-material interface, *Physics of Plasmas* 19 (2012) 056126–156126.